Petroleum Science 20 (2023) 3783–3797

Contents lists available at ScienceDirect

Petroleum Science

journal homepage: www.keaipublishing.com/en/journals/petroleum-science

Original Paper

Study of main factors influencing unsteady-state temperature drop in oil tank storage under dynamic thermal environment coupling

Wei Sun*, Ming-Yang Li, Yu-Duo Liu, Qing-Lin Cheng, Li-Xin Zhao, Shuai Shao, Zhi-Hua Wang

Key Laboratory for Enhancing Oil & Gas Recovery of Ministry of Education, Northeast Petroleum University, Daqing, 163318, Heilongjiang, China

ARTICLE INFO

Article history:
Received 30 October 2022
Received in revised form
20 April 2023
Accepted 4 August 2023
Available online 5 August 2023

Edited by Jia-Jia Fei

Keywords:
Oil temperature drop
Forced convection
Natural convection
Dynamic thermal environment
Quantitative analysis

ABSTRACT

With the increasing oil demand, the construction of oil energy reserves in China needs to be further strengthened. However, given that there has been no research on the main influencing factors of crude oil temperature drop in storage tanks under actual dynamically changing environments, this paper considers the influence of dynamic thermal environment and internal crude oil physical properties on the fluctuating changes in crude oil temperature. A theoretical model of the unsteady-state temperature drop heat transfer process is developed from a three-dimensional perspective. According to the temperature drop variation law of crude oil storage tank under the coupling effect of various heat transfer modes such as external forced convection, thermal radiation, and internal natural convection, the external dynamic thermal environment influence zone, the internal crude oil physical property influence zone, and the intermediate transition zone of the tank are proposed. And the multiple non-linear regression method is used to quantitatively characterize the influence of external ambient temperature, solar radiation, wind speed, internal crude oil density, viscosity, and specific heat capacity on the temperature drop of crude oil in each influencing zone. The results of this paper not only quantitatively explain the main influencing factors of the oil temperature drop in the top, wall, and bottom regions of the tank, but also provide a theoretical reference for oil security reserves under a dynamic thermal environment.

1. Introduction

China's primary energy demand rose 2.1% in 2020, driven by rapid economic recovery from the pandemic (British Petroleum, 2021). Chinese scholars have predicted a 51% increase in China's oil consumption from 2017 to 2026 using a new non-linear dynamic grey model (Wang and Song, 2019). Oil occupies a significant role in all energy consumption, and the development of oil energy reserves is a mandatory step in the construction of a modern energy system in China in the coming period. Meanwhile, the static storage process of crude oil in storage tanks, especially in alpine regions, is affected by dynamic changes in the thermal environment such as solar radiation, atmospheric temperature, wind speed, etc., which causes heat loss of crude oil in tanks and even safety accidents such as condensation of tanks in serious cases. Therefore, to ensure the safety and economic efficiency of storage tanks in the production process, it is essential to accurately grasp the heat transfer and flow law of crude oil in the tanks under the actual dynamic environment.

Numerical simulations are the main method to study the variation of temperature and flow fields in storage tanks (Kocijel et al., 2020; Li et al., 2016; Lin and Armfield, 2005; Zhao et al., 2020; Xue et al., 2023; Wang et al., 2012a). Earlier studies on the numerical simulation of crude oil temperature drop have generally focused on the global large spatial scale of the storage tank, ideally reducing the thermal environment in which the tank is located to a fixed solution condition. Cotter and Charles (1993) found that adding two orders of magnitude to the viscosity at constant viscosity did not significantly change the rate of heat loss during transient natural convection of crude oil in large storage tanks in cold environments. Wang et al. (2005) considered the surrounding and bottom of the tank as adiabatic walls and used the law of energy conservation to establish the heat transfer equation to derive the temperature drop

* Corresponding author.
E-mail address: sunwei19880408@163.com (W. Sun).

https://doi.org/10.1016/j.petsci.2023.08.003

equation for the crude oil in the tank, divided the crude oil into two layers and verified the accuracy of the temperature drop equation with measured data. Li et al. (2019) conducted a numerical simulation of the temperature field of a large floating roof oil reservoir during long-term storage, taking into account the external environment such as constant atmospheric temperature and soil temperature, the physical properties of the oil and the thickness of the insulation layer, and derived the oil temperature variation law and the heat transfer law. The relationship between crude oil temperature drop rate and atmospheric temperature and oil temperature is explained. Meanwhile, previous scholars have mainly focused on the natural convection process of crude oil and the factors related to a crude oil temperature drop from a two-dimensional perspective. Zhao et al. (2014, 2017) studied the temperature distribution during the transient cooling of waxy crude oil in a floating roof storage tank using the finite volume method and analyzed the effect of tank size, the temperature gradient between crude oil and environment, viscosity, and specific heat capacity of crude oil on the cooling rate. Wang et al. (2019) considered the differences in atmosphere, soil, and tank structure on the temperature drop process of single-plate and double-plate floating roof storage tank to investigate and found that the temperature drop rate of single-plate floating roof tank is faster than that of double-plate floating roof tank.

Further, later scholars gradually considered the influence of periodic environment on crude oil, and generally adopted a qualitative approach to analyze the influencing factors of crude oil storage tank temperature drop process. Sun et al. (2018) established a theoretical model of unsteady heat transfer process in large floating roof storage tanks based on two-dimensional periodic boundary conditions, revealing the influence law of ambient temperature, solar radiation and other factors on heat transfer and flow characteristics of crude oil storage tank. Liu et al. (2019, 2020) considered the effect of periodic external temperature on the temperature drop process of crude oil in storage tanks and found that the heat dissipation and cooling rates of top and side walls fluctuated similarly to the external periodic temperature.

In summary, the current study of the unsteady temperature drop process in crude oil storage tanks identifies the surface heat transfer coefficient between the tank and the thermal environment, and the temperature of the thermal environment as a constant value, leading to the heat flow characteristics of the crude oil in the study is following a continuous decay mode. However, in the actual three-dimensional space, the storage tank shows oscillating and fluctuating changes in the heat transfer process of crude oil in the tank due to the influence of dynamically changing coupled boundaries of solar radiation, ambient temperature, and wind speed. And as a result, uneven low-temperature zones are formed within the small spatial scales of the tank top and walls, leading to some deviations between the previous research results and the actual situation. Some scholars have considered the influence of periodic external environment on the temperature drop process of crude oil in storage tanks, but all of them modeled the conclusion from a two-dimensional perspective and analyzed the relevant factors affecting the temperature drop of crude oil from a qualitative perspective without identifying the main influencing factors. Most previous studies have focused on the natural convection process inside crude oil, but few of them have studied the temperature drop of crude oil under the coupling effect of various heat transfer modes such as forced convection, solar radiation, and natural convection generated in real three-dimensional space. Therefore, this paper establishes a theoretical model of the unsteady temperature drop heat transfer process in crude oil storage tank considering the dynamic changes in wind speed, ambient temperature, solar radiation, and other factors. According to the temperature drop variation law of crude oil storage tank coupled with multiple heat transfer modes such as external forced convection, thermal radiation, and internal natural convection, the external dynamic thermal environment influence zone, internal crude oil physical property influence zone, and transition zone of storage tank boundary are proposed. And based on this, a multivariate nonlinear regression method is used to quantitatively characterize the weights of external tank ambient temperature, solar radiation, wind speed, and internal tank crude oil density, viscosity, and specific heat capacity on the temperature drop of crude oil in each influencing region. The related results can provide a reference for the safety reserve of storage tanks under a dynamic thermal environment.

2. Theoretical model of unsteady-state temperature cooling process in crude oil storage tank under dynamic thermal environment coupling

As shown in Fig. 1, heat radiation from the solar and ambient temperature from the outside of the tank to the inside transfer heat to the crude oil, and the soil transfers heat by heat conduction through the tank bottom. In addition, the tanks are subject to forced convection from the wind. The unsteady-state temperature drop of the crude oil storage tank involves various heat transfer coupled processes, so to facilitate the mathematical model solution, the following simplifications are made.

(1) In this paper, the existence of the condensate layer is ignored, and the crude oil in the storage tank is regarded as a single-phase system.
(2) The variation of ambient temperature is mainly expressed by the cosine formula, and the maximum ambient temperature and minimum ambient temperature in this paper are taken as the local monthly average temperature as the reference data of external ambient temperature, ignoring the fluctuation between the daily maximum ambient temperature and minimum ambient temperature.
(3) This paper assumes that the initial temperature distribution of crude oil inside the tank is uniform without a temperature difference.

2.1. Dynamic thermal environment

The tank's top and walls are subject to dynamically changing solar radiation and ambient temperature. The sun does not always shine vertically on the top or walls of the tank during the day. According to Lambert's law, the boundary conditions for the tank top and walls per unit area at any one time are as follows.

Boundary conditions on the tank top:

$$-\lambda_{\mathrm{roof}}\frac{\partial t_{\mathrm{roof}}}{\partial y}=\left(a_{2\mathrm{roof}}+a_{3\mathrm{roof}}\right)\left(t_{\mathrm{en}}-t_{\mathrm{roof}}\right)+I\cdot P_{\mathrm{air}}^{\frac{1}{\cos\theta}}(1+\sigma m_1\ln P_{\mathrm{air}})\cdot\varepsilon_b\cdot\cos\theta\cdot\sin\frac{\pi(\omega T-\omega T_0)}{2(\pi-\omega T_0)},\quad(0\le y\le r_{\mathrm{tank}}) \tag{1}$$

Boundary conditions on the tank wall:

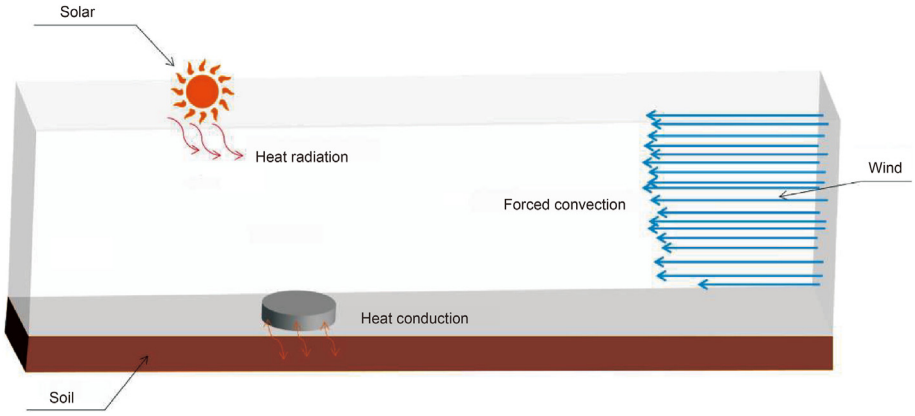

Fig. 1. Theoretical model of unsteady-state temperature cooling heat transfer process in oil storage tank under dynamic thermal environment coupling.

$$-\lambda_{\text{wall}}\frac{\partial t_{\text{wall}}}{\partial z} = (a_{2\text{wall}} + a_{3\text{wall}})(t_{\text{en}} - t_{\text{wall}}) + 2\frac{I \cdot P_{\text{air}}^{\frac{1}{\cos\theta}}(1 + \sigma m_1 \ln P_{\text{air}}) \cdot \varepsilon_{\text{b}}}{\pi} \cdot \left[1 - (1 - \sin\theta)\sin\frac{\pi(\omega T - \omega T_0)}{2(\pi - \omega T_0)}\right], (0 \le z \le h_{\text{tank}}) \tag{2}$$

The tank bottom is primarily associated with soil thermal conductivity, then the tank bottom boundary conditions are:

$$-\lambda_{\text{bott}}\frac{\partial t_{\text{bott}}}{\partial x} = \frac{8\lambda_{\text{soil}}}{2\pi r_{\text{tank}}}(t_{\text{soil}} - t_{\text{bott}}), (0 \le x \le r_{\text{tank}}) \tag{3}$$

where, λ_{roof}, λ_{wall} and λ_{bott} are the thermal conductivity of the top, walls, and tank bottom respectively, x , y , and z are spatial coordinates, m, h_{tank} is the height of the storage tank, m, r_{tank} is the radius of the storage tank, m; $a_{2\text{roof}}$, $a_{2\text{wall}}$ are the convective heat transfer coefficients of the top and walls of the tank, W/(m^2.°C), $a_{3\text{roof}}$, $a_{3\text{wall}}$ are the radiative heat transfer coefficients of the top and wall of the tank respectively, W/(m^2. °C), t_{roof}, t_{wall} and t_{bott} are the boundary temperatures at the tank top, tank wall, and tank bottom, °C, ε_b is the blackness of the tank float, ω is the circle frequency, rad/h, T is the time at the moment, h, T_0 is the time of sunrise, h, I is the solar constant, determined from actual observations, W/m^2, P_{air} is the atmospheric transparency factor, θ is the zenith angle at solar noon, σ is a coefficient related to day length and has a value of 0.346–0.391 when the day length is 8–16 h, m_1 is a factor related to atmospheric mass, $m_1 = \frac{2}{\cos\theta}$.

The periodic pattern of ambient and soil temperatures can be approximated as a cosine function. Thus, the ambient and soil temperatures at any given moment are:

$$t_{\text{en}} = \bar{t}_{\text{en}} - \frac{\Delta t_{\text{en}}}{2}\cos\omega(T - 2) \tag{4}$$

$$t_{\text{soil}} = \bar{t}_{\text{soil}} - \frac{\Delta t_{\text{soil}}}{2}\cos\omega(T - 1) \tag{5}$$

where, t_{en}, t_{en} are the ambient temperature and soil temperature at the moment respectively, °C, $\bar{t}_{\text{en}}$, $\bar{t}_{\text{soil}}$ are the average day and night temperatures of the environment and soil respectively, °C, Δt_{en}, Δt_{soil} are the day-night temperature difference of the environment in 1 day and the day-night temperature difference of the soil in 1 day, respectively, °C.

2.2. Crude oil variable physical parameters

As the external thermal environment changes, the density, thermal conductivity, viscosity, and specific heat capacity of crude oil also change. In this paper, the physical parameters of crude oil at different temperatures were measured using experimental instruments such as a petroleum densitometer, digital rotational viscometer, liquid thermal conductivity tester, crude oil rheometer, and differential scanning calorimetry. And the measured data were fitted to obtain the density, thermal conductivity, viscosity, and specific heat equations of crude oil as Eqs. (6)–(9). Crude oil density and thermal conductivity vary negatively and linearly with temperature, while viscosity varies as a power function of temperature and specific heat capacity increases and then decreases as oil temperature decreases. The specific crude oil variability model is shown below.

Density of crude oil:

$$\rho = \rho_{20}[1 - 0.00061(t_{\text{oil}} - 20)] \tag{6}$$

Thermal conductivity of crude oil:

$$\lambda = \frac{116.5}{\rho_{20}}(1 - 0.00054t_{\text{oil}}) \tag{7}$$

Viscosity of crude oil:

$$\mu = e\text{^}[-27.8 + 8803.7/(t_{\text{oil}} + 273.15)] \tag{8}$$

Specific heat capacity of crude oil:

$$c = 0.0398t_{\text{oil}}^3 - 3.8645t_{\text{oil}}^2 + 90.369t_{\text{oil}} + 2363.5 \tag{9}$$

where, t_{oil} is the temperature of crude oil, °C, ρ is the density of crude oil, kg/m^3, ρ_{20} is the density of crude oil at 20 °C, kg/m^3, λ is the thermal conductivity of crude oil, W·(m·°C)$^{-1}$, μ is the viscosity of crude oil, Pa·s, c is the specific heat capacity, J·(kg·°C)$^{-1}$.

2.3. Control equations

Based on the physical parameters of the crude oil, the heat transfer and flow processes of the crude oil are described by establishing the corresponding control equations. $k-\varepsilon$ turbulence model is used to simulate the vortex motion during the temperature drop of the crude oil in the storage tank (Huang et al., 2020; Liu and Chung, 2012; Pasley and Clark, 2000; Zhang et al., 2008; Sun et al., 2023; Wang and Lin, 2020; Wang et al., 2012b).

The mass equation:

$$\frac{\partial \rho}{\partial t}+\frac{\partial(\rho u)}{\partial x}+\frac{\partial(\rho v)}{\partial y}+\frac{\partial(\rho w)}{\partial z}=0 \tag{10}$$

where, t is the unsteady-state heat transfer time, s, x, y and z are the spatial coordinates, m, u, v, and w are the velocity components in the x, y and z directions, respectively, m/s^2.

The momentum equation:

$$\frac{\partial(\rho u)}{\partial t}+\frac{\partial(\rho u u)}{\partial x}+\frac{\partial(\rho v u)}{\partial y}+\frac{\partial(\rho w u)}{\partial z}=-\frac{\partial P}{\partial x}+\mu\left(\frac{\partial^2 u}{\partial x^2}+\frac{\partial^2 v}{\partial y^2}+\frac{\partial^2 w}{\partial z^2}\right) \tag{11}$$

$$\frac{\partial(\rho v)}{\partial t}+\frac{\partial(\rho u v)}{\partial x}+\frac{\partial(\rho v v)}{\partial y}+\frac{\partial(\rho w v)}{\partial z}=-\frac{\partial P}{\partial y}+\mu\left(\frac{\partial^2 v}{\partial x^2}+\frac{\partial^2 v}{\partial y^2}+\frac{\partial^2 v}{\partial z^2}\right)-\rho g \tag{12}$$

$$\frac{\partial(\rho w)}{\partial t}+\frac{\partial(\rho u w)}{\partial x}+\frac{\partial(\rho v w)}{\partial y}+\frac{\partial(\rho w w)}{\partial z}=-\frac{\partial P}{\partial z}+\mu\left(\frac{\partial^2 w}{\partial x^2}+\frac{\partial^2 w}{\partial y^2}+\frac{\partial^2 w}{\partial z^2}\right) \tag{13}$$

where, P is the hydrostatic pressure of the crude oil, Pa, g is the acceleration of gravity, m/s^2.

The energy equation:

$$\frac{\partial(\rho t_{\mathrm{oil}})}{\partial t}+\frac{\partial(\rho u t_{\mathrm{oil}})}{\partial x}+\frac{\partial(\rho v t_{\mathrm{oil}})}{\partial y}+\frac{\partial(\rho w t_{\mathrm{oil}})}{\partial z}=\frac{\lambda}{c}\left(\frac{\partial^2 t_{\mathrm{oil}}}{\partial x^2}+\frac{\partial^2 t_{\mathrm{oil}}}{\partial y^2}+\frac{\partial^2 t_{\mathrm{oil}}}{\partial z^2}\right) \tag{14}$$

The turbulence equation:

$$\rho\frac{\mathrm{d}k}{\mathrm{d}t}=\frac{\partial}{\partial x}\left[\left(\mu+\frac{\mu_{\mathrm{t}}}{\sigma_{\mathrm{k}}}\right)\frac{\partial k}{\partial x}\right]+\frac{\partial}{\partial y}\left[\left(\mu+\frac{\mu_{\mathrm{t}}}{\sigma_{\mathrm{k}}}\right)\frac{\partial k}{\partial y}\right]+\frac{\partial}{\partial z}\left[\times\left(\mu+\frac{\mu_{\mathrm{t}}}{\sigma_{\mathrm{k}}}\right)\frac{\partial k}{\partial z}\right]+G_{\mathrm{k}}+G_{\mathrm{b}}-\rho\varepsilon \tag{15}$$

$$\rho\frac{\mathrm{d}\varepsilon}{\mathrm{d}t}=\frac{\partial}{\partial x}\left[\left(\mu+\frac{\mu_{\mathrm{t}}}{\sigma_{\varepsilon}}\right)\frac{\partial \varepsilon}{\partial x}\right]+\frac{\partial}{\partial y}\left[\left(\mu+\frac{\mu_{\mathrm{t}}}{\sigma_{\varepsilon}}\right)\frac{\partial \varepsilon}{\partial y}\right]+\frac{\partial}{\partial z}\left[\times\left(\mu+\frac{\mu_{\mathrm{t}}}{\sigma_{\varepsilon}}\right)\frac{\partial \varepsilon}{\partial z}\right]+\mathrm{C}_{1\varepsilon}\frac{\varepsilon}{k}(G_{\mathrm{k}}+\mathrm{C}_{3\varepsilon}G_{\mathrm{b}})-\mathrm{C}_{2\varepsilon}\rho\frac{\varepsilon^2}{k} \tag{16}$$

$$\mu_{\mathrm{t}}=\rho\mathrm{C}_{\mu}\frac{k^2}{\varepsilon} \tag{17}$$

where, μ_{t} is the turbulent viscosity coefficient, G_{K} denotes the turbulent energy due to the mean velocity gradient, G_{b} is the turbulent energy due to the buoyancy. C_{μ}, $C_{1\varepsilon}$, $C_{2\varepsilon}$,and $\mathrm{C}_{3\varepsilon}$ are constant term coefficients of 0.09, 1.44, 1.92, 1.11, respectively. σ_k and σ_ε are the turbulent Prandtl numbers of turbulent energy k and dissipation rate ε, respectively.

3. Numerical simulation of temperature cooling processes in crude oil storage tank

3.1. Theoretical model validation

As shown in Fig. 2, the grid includes the airflow area and the crude oil storage tank area, and the overall model grid number is 10720000. Considering the wind speed, solar radiation, ambient temperature, and the complex heat exchange process of the crude oil in the tank in three dimensions therefore the calculation is done with a double precision solver. The velocity inlet and pressure outlet are set to simulate the wind flow process. In order to make the model converge better, the pressure-velocity coupling algorithm of SIMPLEC is used, and the pressure term is set to second order format. And the flow control equations are chosen in second order upwind discrete format to obtain more accurate results. The convergence of the calculation is judged by the residual values of the continuity equation and momentum equation less than 10^{-3} and the residual values of the energy equation less than 10^{-6} (Li et al., 2019; Seddegh et al., 2015; Wang et al., 2020).

In order to verify the accuracy of the model, the VITO MTT system was used in this study to monitor the process of the crude oil temperature drop on day 4 at locations 0.5, 1.6, 10.2, and 18.5 m from the bottom of the tank inside the 100,000 m^3 floating roof storage tank in winter with an initial outside wind speed of 0.9 m/s. As shown in Fig. 3, the temperature drop of the crude oil under the dynamic thermal environment shows a fluctuating variation inside the top and bottom of the tank. The closer the tank top boundary, the greater the relative error, with the highest relative error of 10.58% between the simulated oil temperature data and the actual measured value at 18.5 m, since the external wind velocity during the actual tank crude oil temperature drop shows irregular fluctuation changes, which is different from the simulated wind velocity. Also, the amount of solar radiation received per unit area of the tank varies depending on factors such as solar altitude angle and cloud thickness, resulting in a large error at the tank top. The closer to the closed bottom space of the tank, the smaller the error, with an average relative error of 0.02% between the simulated and measured oil temperature values at the bottom. In general, the temperature drop simulation process is similar to the actual temperature drop variation trend, and the overall relative error is 0.05%, which proves the accuracy of the mathematical model and simulation method in this paper.

3.2. Heat transfer and flow characteristics of crude oil storage tank temperature drop

In this paper, a 10×10^4 m^3 crude oil storage tank is used as an example to simulate the temperature drop pattern of crude oil under the dynamic thermal environment of wind speed, ambient temperature, and solar radiation, and the specific external environment of the storage tank and physical parameters of crude oil are shown in Table 1.

As shown in Fig. 4, the wind sweeping across the top plate of the tank brings forced convection, while convective heat transfer in the form of bypass flow is formed at the tank wall. Due to the wind direction, the windward and leeward sides of the tank wall are affected by convective heat transfer to a different extent, resulting in significant changes in the internal crude oil heat transfer and flow state. Hence the analysis of the tank wall is divided into leeward and windward sides.

As shown in Fig. 5, the tank top is affected by wind speed forced convection, solar radiation and ambient temperature conduction, etc., and the crude oil at the top of the tank first warms down. The wind bypasses both sides of the tank wall and forms a turbulent vortex structure. With the increase of time, the turbulent vortex structure on the leeward side matures, the convection coefficient increases, and the temperature drop of crude oil on the leeward side accelerates. This leads to the increase of crude oil density and viscosity, and the overall flow rate is lower than that of the windward side.

As shown in Fig. 6(d), at a wind speed of 0 m/s, the temperature drop at the tank top on the windward side is more pronounced than

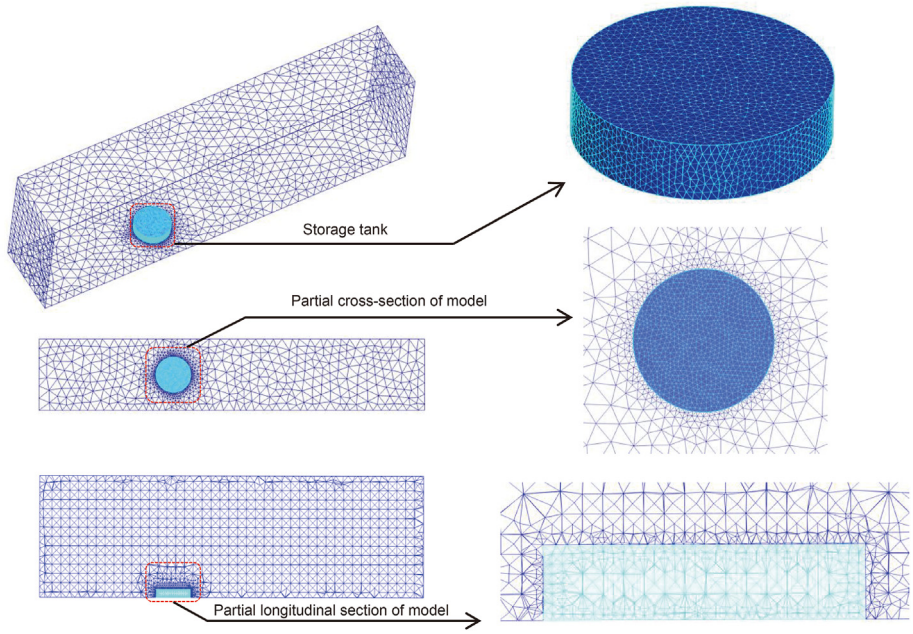

Fig. 2. Model grid.

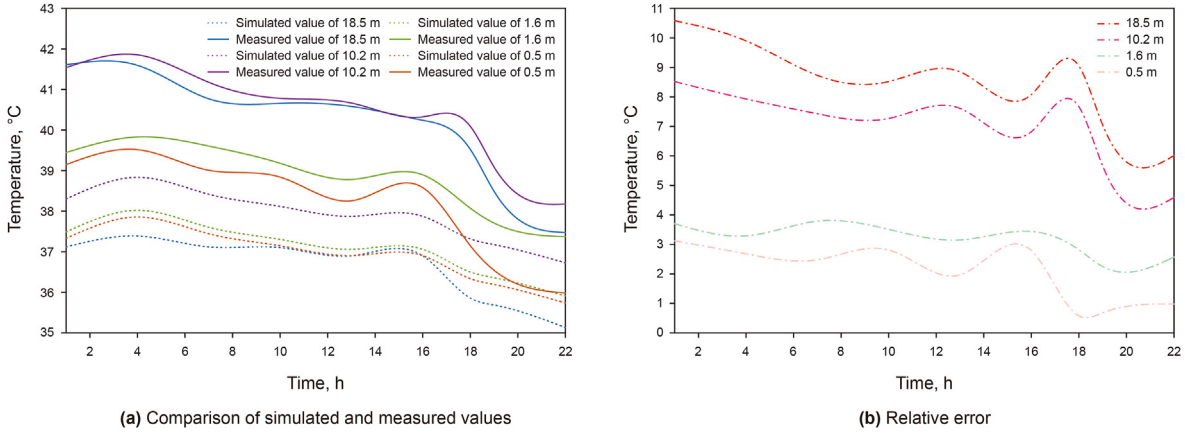

(a) Comparison of simulated and measured values

(b) Relative error

Fig. 3. Comparison of simulated and measured oil temperature values and relative error diagrams.

Table 1
Parameters of the external environment of the storage tank and the physical properties of the crude oil.

Item	Values	Item	Values
Tank diameter, m	80	Maximum environment temperature, °C	4
Tank height, m	19	Minimum environment temperature, °C	−4
Blackness	0.96	Initial temperature of crude oil in tank, °C	50
Wind speed, m/s	0.9, 0.5, 0	Soil thermal conductivity, W/(m·°C)	2.75
Thickness of the insulating materials, m	0.08	Heat flux from solar radiation, W/m^2	60~240
Atmospheric transparency factor	0.7–0.8	Density of oil at 20 °C, kg/m^3	0.86
Solar constant, W/m^2	1367	Viscosity of oil at 20 °C, Pa·s	4.97
Thermal conductivity of the insulating materials, W/(m·°C)	0.037	Thermal conductivity of oil at 20 °C, W/(m·°C)	0.246
Declination, °	−23.25	Specific heat capacity of oil at 20 °C, J/(kg·°C)	2989

on the leeward side. However, as the wind speed increases near the top and leeward side of the tank, forced convection is enhanced, and the temperature drop rate at the tank top on the leeward side accelerates. Similarly, on the center side of the tank, as the wind speed increases, the temperature drop at the tank top is faster, and more low-temperature zones appear, as in Fig. 6(b). The tank bottom also experiences a transitional layer of temperature drop due to the accumulation of cold oil and heat transfer to the soil, which results in faster heat loss. The three conditions show that the temperature drop is more pronounced as the wind speed increases, resulting in stronger forced convection at the tank top.

The variation in temperature of the top and tank bottom and the walls in space is shown in Figs. 7–10.

As shown in Fig. 7, the crude oil temperature distribution

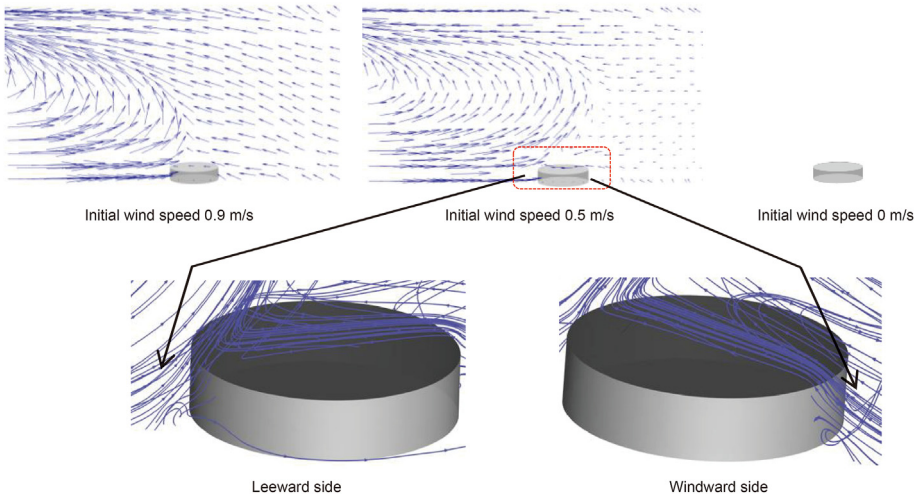

Fig. 4. Vector diagram of different wind speeds.

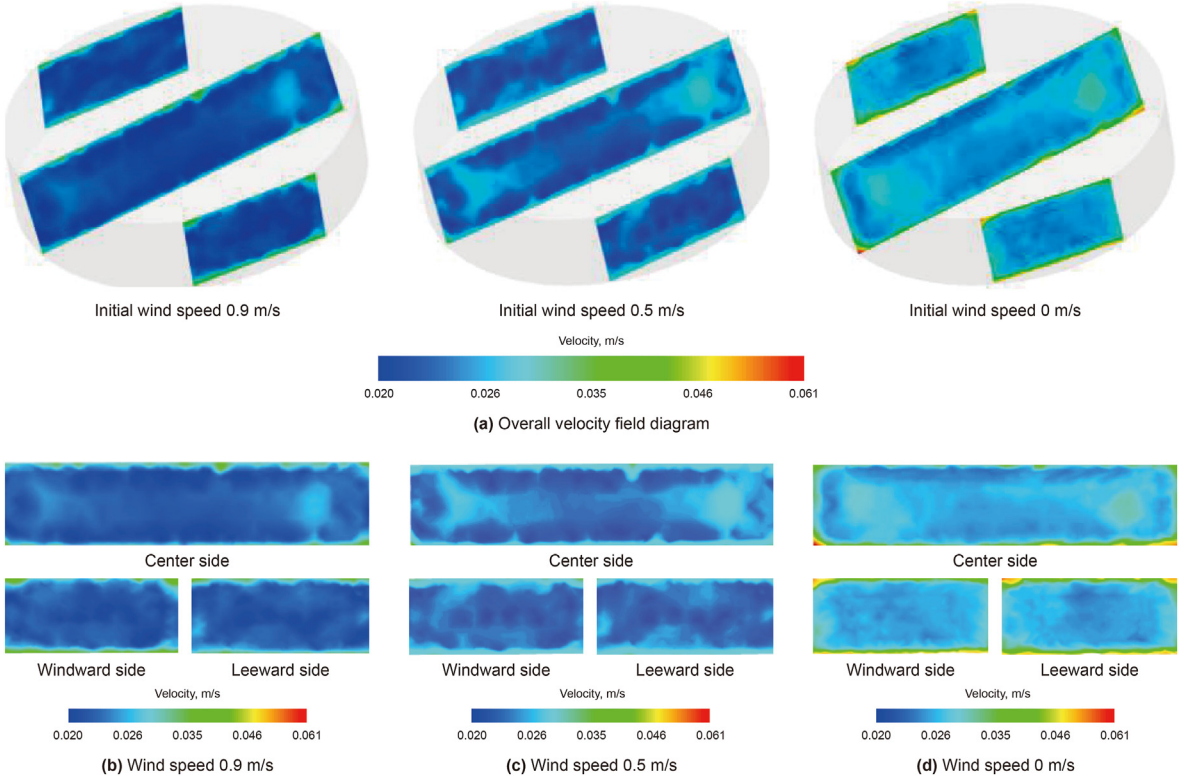

Fig. 5. Velocity field after day 4 of temperature drop, with initially different wind speeds.

patterns for the three operating conditions within 16.6–19 m at the tank top are near identical. The crude oil at 19 m at the tank top has the lowest temperature, higher viscosity, and weaker fluidity. With the increase in wind speed, the temperature drop rate at the tank top is obviously accelerated, and the fluctuation of crude oil temperature increases. The fluctuation of crude oil temperature at the tank top 17.4–18.6 m with wind speeds of 0.9 and 0.5 m/s is about 0.5 and 0.1 °C, respectively, while the temperature fluctuation at the same area location without wind speed is only about 0.01 °C. The temperature stabilizes when the level is lowered from 17.4 to 16.6 m, indicating that the crude oil in this area is less affected by external influences.

Temperature fluctuations are more obvious near the tank bottom. The closer to the tank bottom, the lower the oil temperature within 0.5 m, with fluctuations of 0.15 °C from 0.5 to 1.5 m. The temperature at the bottom 2–2.5 m was basically the same.

The overall temperature change between the leeward and windward sides of the tank wall is small due to the effect of the insulation layer. Under the influence of wind speed, ambient temperature, and solar radiation, the oil temperature at the 40 m boundary between the leeward and windward sides of the tank wall is the lowest in Figs. 9(a) and Fig. 10(a), with the average temperature remaining at 4.2 and 4.6 °C at 0.9 and 0.5 m/s wind speeds respectively. The temperature distribution of crude oil on

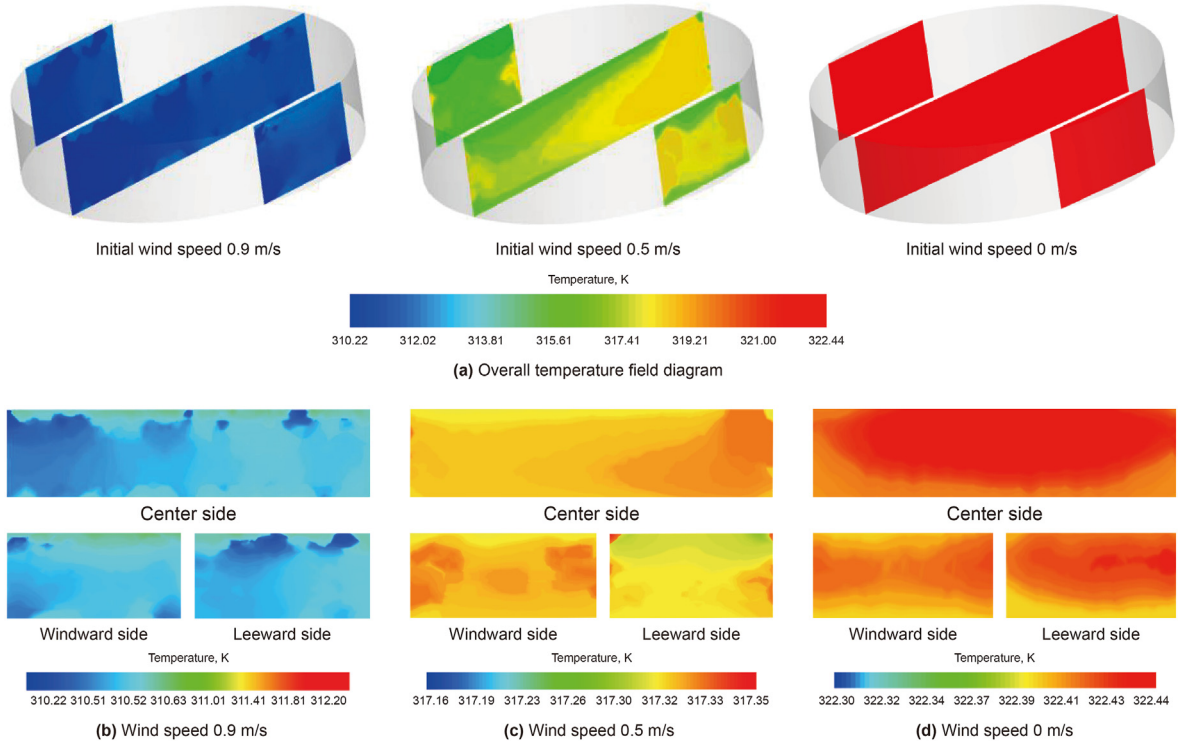

Fig. 6. Temperature field after day 4 of temperature drop, with initially different wind speeds.

the leeward and windward sides of the tank wall at no wind speed was similar and stable. As the wind speed increases, the maximum temperature difference between the crude oil at 39–39.5 m on the leeward side and the boundary at 40 m is approximately 33.8 °C, while that on the windward side is around 33.4 °C. It can be seen that the temperature drop rate at the boundary of the tank wall on the leeward side is faster than that on the windward side. The temperature of the crude oil within a radius of 38 m remains relatively stable.

4. Quantitative characterization of the main factors influencing the temperature cooling process in crude oil storage tank

This paper uses a multivariate non-linear regression approach to quantify the main influences that lead to changes in crude oil temperature. The Levenberg-Marquardt algorithm is suitable for solving multivariate non-linear problems. It is an improvement on the gradient descent and Newton iteration methods, being faster than the gradient descent method and more stable than the Newton iteration method (Wilamowski and Irwin, 2018). This experiment simulates the temperature drop process for 4 days. Among the raw data in the nonlinear regression include oil temperature, wind speed, solar radiation, ambient temperature, atmospheric temperature, soil temperature, density, viscosity, and specific heat capacity near the top, bottom, and walls of the tank with inlet wind speeds of 0.9, 0.5, and 0 m/s, respectively. The main steps are as follows.

(1) Normalization: In order to reduce errors in the analysis results due to differences in magnitudes between the external dynamic thermal environment, the variable physical parameters of the crude oil, and the boundary crude oil temperature, the raw data is normalized so that the pre-processed data is limited to the same characteristics as the raw data between 0 and 1.

$$x^* = \frac{x - \min}{\max - \min} \tag{18}$$

(2) Development of the target mathematical model: Crude oil temperature is used as the dependent variable in the study, with the external factors ambient temperature, solar radiation, wind speed, and soil temperature and the internal factors crude oil density, viscosity, and specific heat capacity as independent variables. The influences on the variation of crude oil temperature involve the action of both internal and external influences, and their weights are combined with the sum of the product of the powers of the corresponding sample data plus a constant term to form a multivariate non-linear expression.

$$f(x) = C + \sum_{N=1}^{n} \sum_{j=1}^{n} a_{N,j-1} x_{i,N}^{j} \tag{19}$$

(3) Numerical iterative solution of the Levenberg-Marquardt algorithm:
① Given an initial value x_0 and an initialization radius U_r. i takes the value of the number of independent variables.
② For the N th iteration, add the trust region to the Gauss-Newton method to solve for:

$$\min \frac{1}{2} \left\| f(x_N) + J(x_N)^T \Delta x_N \right\|^2, s.t. \quad \|D_m \Delta x_N\|^2 \le U_r \tag{20}$$

where, U_r is the radius of the trust region and D_m is the coefficient matrix.

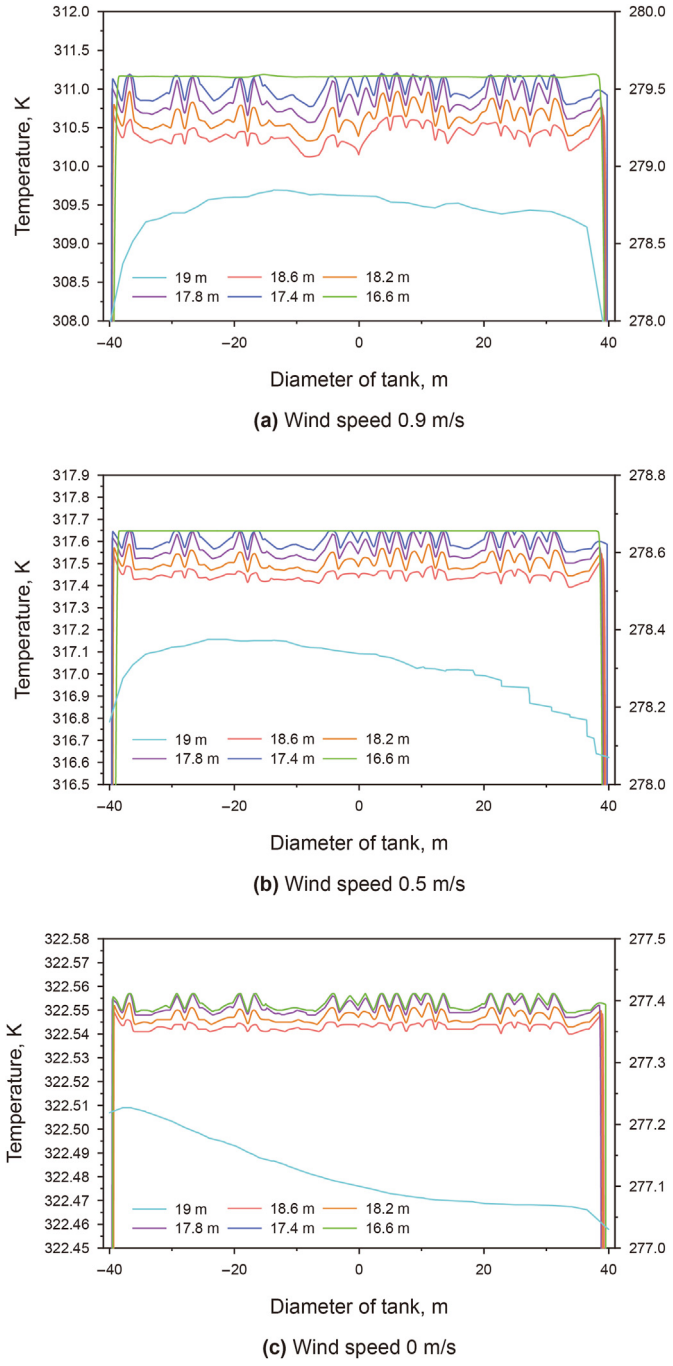

Fig. 7. Temperature distribution chart of the tank top.

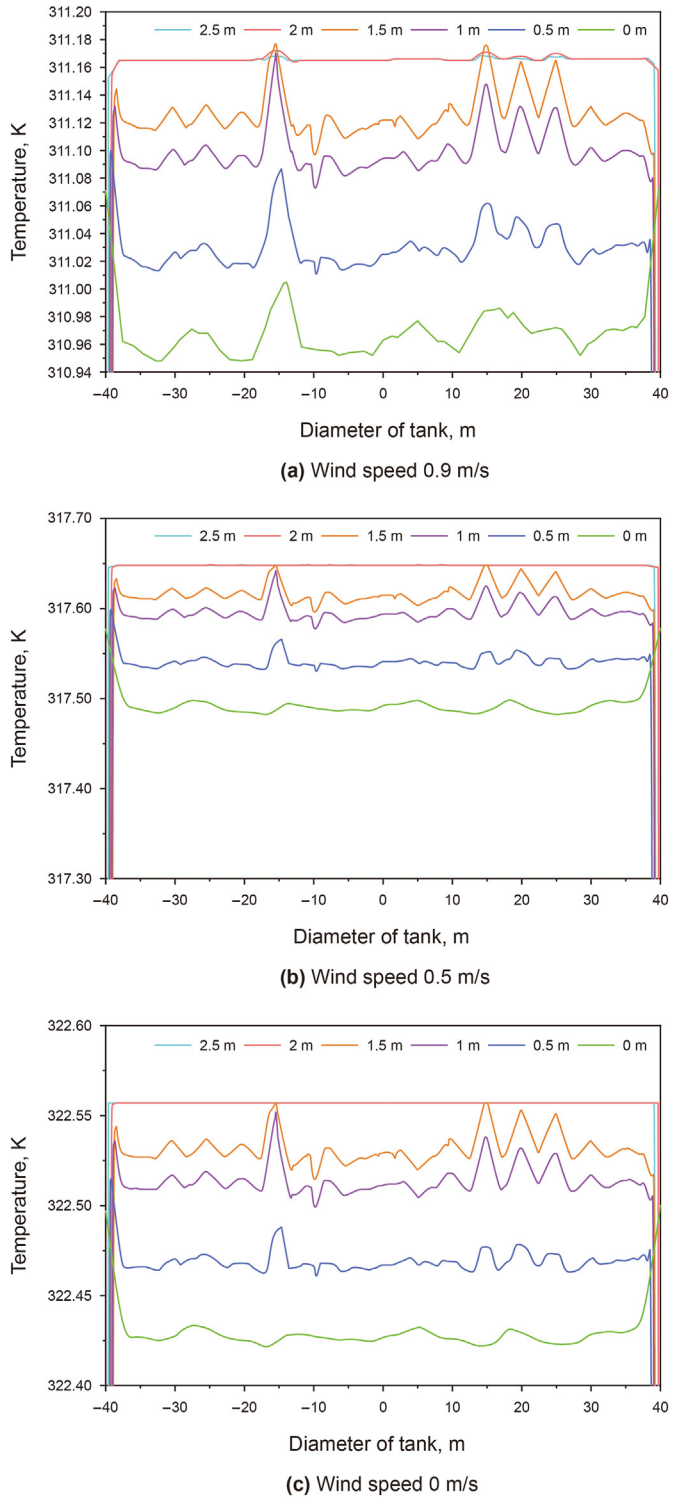

Fig. 8. Temperature distribution chart of the tank bottom.

③ Calculation of trust area, F.

$$F = \frac{f(x+\Delta x) - f(x)}{J(x)^T \Delta x} \tag{21}$$

④ If $> \frac{3}{4}$, then $r = 2r$.

⑤ If $< \frac{1}{4}$, then $r = \frac{1}{2}r$.

⑥ If F is greater than a certain threshold, the approximation is considered feasible and

$$x_{N+1} = x_N + \Delta x_N \tag{22}$$

⑦ Determine if the algorithm converges. If it does not converge then return to step ②, otherwise end the iteration.

(4) Judging the goodness of fit.

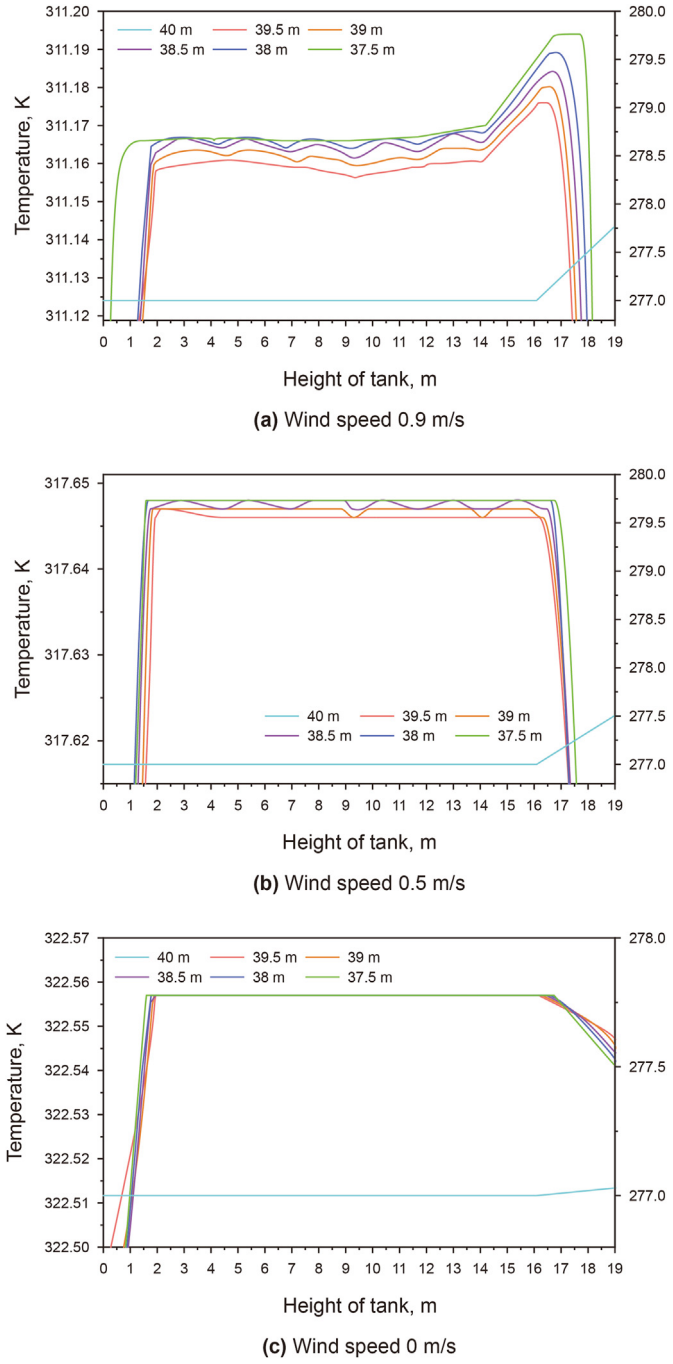

Fig. 9. Temperature distribution chart of the tank's leeward side.

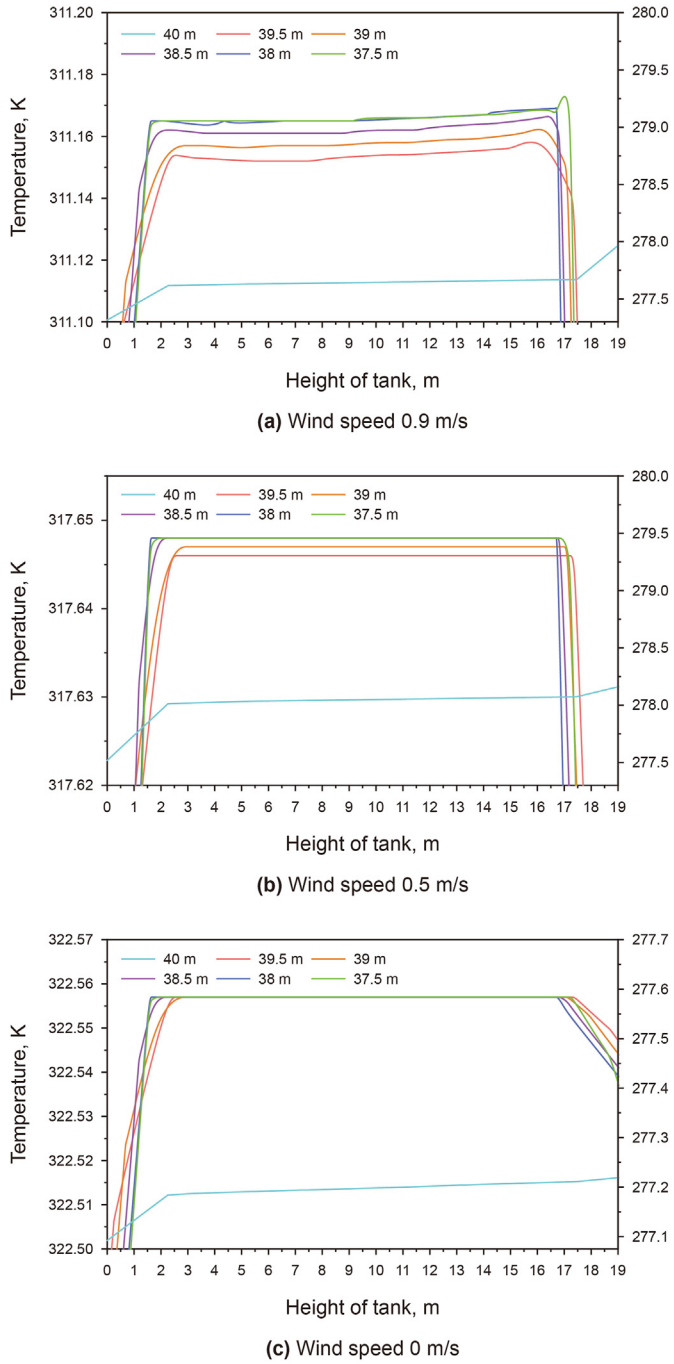

Fig. 10. Temperature distribution chart of the tank's windward side.

$$R^2 = 1 - \frac{SS_{\text{res}}}{SS_{\text{tot}}} = 1 - \frac{\sum_{i=1}^{n} (y_i - f_i)^2}{\sum_{i=1}^{n} \left(y_i - \frac{1}{n} \sum_{i=1}^{n} y_i \right)^2} \tag{23}$$

A fitted equation with a goodness of fit greater than 0.9 close to 1 was selected to characterize the relationship between crude oil temperature and internal crude oil physical influences and external environmental influences.

Based on the variation pattern of crude oil temperature drop in different spatial areas of the tank, combined with the weighting analysis of the main factors leading to the temperature drop, the external dynamic thermal environment influence zone, the internal crude oil physical property influence zone, and the transition zone can be further defined reasonably. The oil temperature at the top, bottom, leeward, and windward sides of the storage tank is multivariate and nonlinearly fitted to the external environmental factors and the internal crude oil physical properties. t_{oil} means oil temperature, C denotes random error, V_{roof} indicates the wind speed at the tank top, V_{F} indicates wind speed on the windward side, V_{B} indicates wind speed on the leeward side, t_{en} means

ambient temperature, t_{soil} means soil temperature, q_{sroof} represents solar radiation at the tank top, q_{swall} represents solar radiation at the tank wall, ρ denotes density, μ denotes viscosity, c represents specific heat capacity. In the model, the coefficients of a_1 to a_6, b_1 to b_6 , and x_1 to x_5 indicate the magnitude of the weights of external or internal factors respectively, i.e., the fitting coefficients. Therefore, to facilitate the discussion of the main influencing factors, the powers in each nonlinear regression model are the same. The power of wind speed 0.9 m/s at the tank top: k_{roof1}, the power of wind speed 0.5 m/s at the tank top: k_{roof2}, the power of wind speed 0 m/s at the tank top: k_{roof3}, the power of wind speed 0.9 m/s at the tank bottom: k_{bott1}, the power of wind speed 0.5 m/s at the tank bottom: k_{bott2}, the power of wind speed 0 m/s at the tank bottom: k_{bott3}. And the power of the leeward and windward sides is expressed in the same way as above. The details are shown in Table 2. The fitting coefficients of the factors influencing the oil temperature at each position are shown in Tables 3–6.

According to the spatial distribution characteristics of the temperature of crude oil in the tank, the zone of influence of the thermal environment of crude oil in the tank is defined as the zone influenced by external wind speed, solar radiation, and ambient temperature as the main external influence (III), the zone influenced by crude oil density, viscosity and specific heat capacity as the main internal influence (I), and the intermediate transition zone (II).

At the tank top, the thickness of the external influence zone (III) increases from 0.2 to 0.65 m. The thickness of the internal influence zone (I) shortens from 1.4 to 0.9 m with the increase in wind speed, indicating that the increase of wind speed accelerates the process of crude oil temperature drop by coupled heat transfer such as forced convection and solar radiation. As in Fig. 11(a) and (b), the storage tank level 18.35–19 m, 18.65–19 m were formed by the wind sweeping across the flat plate with forced convection as the main, and solar radiation, ambient temperature thermal conductivity as the secondary external environmental impact zone, the external conditions accounted for more than 70%, of which the wind speed is the main impact factor weighting nearly 50%. When the liquid level drops to the area below 17.5 or 17.9 m, respectively, the internal influence zone (I) is where natural convection is the main mode of heat transfer, with the most important influence factor being the density of crude oil, which accounts for over 60% of the weight. The thickness of the intermediate transition zone (II) is 0.75–0.85 m, and the weights of wind speed, and ambient temperature fluctuate with the weights of internal crude oil density and specific heat capacity.

As in Fig. 12, an external soil influence zone (III) with a thickness of 0.19–0.46 m was formed at the bottom of the tank, and the soil temperature influence weight was between 40% and 60%, and this zone was mainly dominated by the soil heat conduction of the crude oil to the external low temperature. As in Fig. 12(a) and (b), the internal influence zone (I) with a thickness of 1.04–1.3 m, with density as the main influence factor, indicates that natural convection caused by the density difference of crude oil is the main heat transfer mode in this region. The specific heat capacity is the main influencing

Table 2
Non-linear regression model for the influence of oil temperature on the top, bottom, leeward side of the tank wall and windward side of the tank wall.

Location	Wind speed, m/s	Non-linear regression model
Tank top	0.9	$t_{oil} = C + a_1 V_{roof}{}^{k_{roof1}} + a_2 t_{en}{}^{k_{roof1}} + a_3 q^{sroof^{k_{roof1}}} + a_4 \rho^{k_{roof1}} + a_5 \mu^{k_{roof1}} + a_6 c^{k_{roof1}}$
	0.5	$t_{oil} = C + b_1 V_{roof}{}^{k_{roof2}} + b_2 t_{en}{}^{k_{roof2}} + b_3 q_{sroof}{}^{k_{roof2}} + b_4 \rho^{k_{roof2}} + b_5 \mu^{k_{roof2}} + b_6 c^{k_{roof2}}$
	0	$t_{oil} = C + x_1 t_{en}{}^{k_{roof3}} + x_2 q_{sroof}{}^{k_{roof3}} + x_3 \rho^{k_{roof3}} + x_4 \mu^{k_{roof3}} + x_5 c^{k_{roof3}}$
Tank bottom	0.9	$t_{oil} = C + a_1 t_{soil}{}^{k_{bott1}} + a_2 \rho^{k_{bott1}} + a_3 \mu^{k_{bott1}} + a_4 c^{k_{bott1}}$
	0.5	$t_{oil} = C + b_1 t_{soil}{}^{k_{bott2}} + b_2 \rho^{k_{bott2}} + b_3 \mu^{k_{bott2}} + b_4 c^{k_{bott2}}$
	0	$t_{oil} = C + x_1 t_{soil}{}^{k_{bott3}} + x_2 \rho^{k_{bott3}} + x_3 \mu^{k_{bott3}} + x_4 c^{k_{bott3}}$
Leeward side of tank wall	0.9	$t_{oil} = C + a_1 V_B{}^{k_{B1}} + a_2 t_{en}{}^{k_{B1}} + a_3 q_{swall}{}^{k_{B1}} + a_4 \rho^{k_{B1}} + a_5 \mu^{k_{B1}} + a_6 c^{k_{B1}}$
	0.5	$t_{oil} = C + b_1 V_B{}^{k_{B2}} + b_2 t_{en}{}^{k_{B2}} + b_3 q_{swall}{}^{k_{B2}} + b_4 \rho^{k_{B2}} + b_5 \mu^{k_{B2}} + b_6 c^{k_{B2}}$
	0	$t_{oil} = C + x_1 t_{en}{}^{k_{B3}} + x_2 q_{swall}{}^{k_{B3}} + x_3 \rho^{k_{B3}} + x_4 \mu^{k_{B3}} + x_5 c^{k_{B3}}$
Windward side of tank wall	0.9	$t_{oil} = C + a_1 V_F{}^{k_{F1}} + a_2 t_{en}{}^{k_{F1}} + a_3 q_{swall}{}^{k_{F1}} + a_4 \rho^{k_{F1}} + a_5 \mu^{k_{F1}} + a_6 c^{k_{F1}}$
	0.5	$t_{oil} = C + b_1 V_F{}^{k_{F2}} + b_2 t_{en}{}^{k_{F2}} + b_3 q_{swall}{}^{k_{F2}} + b_4 \rho^{k_{F2}} + b_5 \mu^{k_{F2}} + b_6 c^{k_{F2}}$
	0	$t_{oil} = C + x_1 t_{en}{}^{k_{F3}} + x_2 q_{swall}{}^{k_{F3}} + x_3 \rho^{k_{F3}} + x_4 \mu^{k_{F3}} + x_5 c^{k_{F3}}$

Table 3
Non-linear regression fit coefficients for factors influencing oil temperature of the tank top.

Wind speed, m/s	Height, m	Random error	Power	Wind speed at tank top	Ambient temperature	Solar radiation	Density	Viscosity	Specific heat capacity	R^2
0.9	19	0.993	0.922	−2.576	0.789	0.789	0.087	0.05	0.003	0.989
	18.6	0.502	2.128	−0.74	0.566	0.284	−0.162	−0.02	−0.068	0.997
	18.2	2.016	1.008	−1	−0.989	−0.121	−0.626	−0.397	0.095	0.996
	17.8	0.787	1.2	−0.811	0.566	−0.713	0.265	0.251	0.213	0.992
	17.4	0.791	1.63	−0.308	0.272	0.178	−0.628	−0.287	0.032	0.991
	16.6	0.767	1.371	0.04	0.019	0.009	−0.715	−0.111	0.224	0.998
0.5	19	0.513	1.75	−0.769	0.288	0.255	−0.03	0.091	0.199	0.995
	18.6	1.034	1.074	−0.58	−0.482	0.172	−0.068	−0.386	0.275	0.997
	18.2	0.434	1.589	−0.604	0.45	0.391	0.145	0.224	−0.274	0.983
	17.8	0.332	1.009	0.411	0.5	0.498	−0.57	−0.669	0.171	0.989
	17.4	0.431	0.851	1.159	−0.665	−0.827	−15.76	14.866	1.456	0.991
	16.6	0.767	1.371	0.04	0.019	0.009	−0.715	−0.111	0.224	0.993
0	19	0.99	0.973	–	−0.593	−0.415	0.001	0.055	0.011	0.989
	18.6	0.516	1.886	–	−0.438	−0.604	0.23	0.296	0.484	0.986
	18.2	−0.331	0.923	–	0.1	0.126	0.228	0.101	1.203	0.993
	17.8	0.403	2.761	–	0.06	−0.038	−0.261	−0.145	0.635	0.999
	17.4	0.481	3.865	–	0.1	−0.034	−0.215	−0.374	0.564	0.999
	16.6	0.483	3.69	–	0.09	−0.03	−0.236	−0.346	0.557	0.999

Table 4
Non-linear regression fit coefficients for factors influencing oil temperature of the tank bottom.

Wind speed, m/s	Height, m	Random error	Power	Soil temperature	Density	Viscosity	Specific heat capacity	R^2
0.9	2.5	0.061	1.104	0.1	5.919	−6.021	0.941	0.979
	2	0.059	1.105	0.1	5.956	−6.056	0.943	0.983
	1.5	0.103	1.115	0.1	5.519	−5.661	0.899	0.997
	1	0.792	1.695	0.004	−1.689	0.891	0.208	0.998
	0.5	0.805	1.366	−0.471	0.664	−0.172	−0.648	0.998
	0	1.399	3	−5	0.5	−1.913	4.375	0.999
0.5	2.5	−0.295	1.415	0.1	10.85	−10.55	1.303	0.991
	2	−0.368	1.386	0.1	11.502	−11.13	1.376	0.986
	1.5	0.572	1.683	0.005	−0.371	−0.202	0.427	0.993
	1	0.59	1.627	0.272	−0.423	−0.167	0.137	0.995
	0.5	0.589	1.633	0.206	−0.428	−0.16	0.205	0.999
	0	−0.001	0.721	0.571	−0.004	−0.042	0.435	0.999
0	2.5	0.515	1.903	0.001	−0.292	−0.223	0.485	0.997
	2	0.515	1.904	0.001	−0.307	−0.208	0.485	0.997
	1.5	0.509	1.963	0.005	−0.3	−0.211	0.492	0.986
	1	0.506	1.947	0.005	−0.3	−0.207	0.494	0.998
	0.5	0.517	1.891	0.241	−0.289	−0.228	0.242	0.993
	0	0.188	1.289	1.669	0.1	−0.227	−0.843	0.998

Table 5
Non-linear regression fit coefficients for factors influencing oil temperature of the tank's leeward side.

Wind speed, m/s	Radius, m	Random error	Power	Wind speed at tank wall	Ambient temperature	Solar radiation	Density	Viscosity	Specific heat capacity	R^2
0.9	40	0.589	2.691	−1.773	0.108	−0.129	0.017	1.167	0.54	0.986
	39.5	0.599	2.682	−1.804	0.102	−0.124	0.007	1.198	0.525	0.988
	39	−0.613	0.992	21.02	−0.942	−1	3.381	−23.016	2.616	0.995
	38.5	0.591	2.69	−0.354	0.107	−0.128	−1.35	1.113	0.537	0.991
	38	0.592	2.69	−0.355	0.107	−0.128	−1.351	1.114	0.536	0.975
	37.5	0.592	2.69	−0.356	0.107	−0.128	−1.35	1.114	0.536	0.988
0.5	40	0.522	3.478	−0.675	0.1	−0.028	0.244	−0.198	0.521	0.989
	39.5	0.863	1.007	−0.334	0.1	0.1	−0.603	−0.025	0.037	0.991
	39	0.488	3.147	0.33	0.1	−0.02	0.414	−1.339	0.547	0.974
	38.5	0.243	1.331	−0.5	0.1	0.059	7.034	−7.383	0.699	0.975
	38	−0.045	1.254	−0.373	0.1	0.054	9.79	−9.846	0.998	0.987
	37.5	0.22	1.108	−0.032	0.1	0.096	2.934	−3.254	0.685	0.992
0	40	0.595	0.974	–	−0.1	−0.125	−0.418	−0.177	0.53	0.945
	39.5	0.412	2.68	–	0.053	−0.033	−0.297	−0.117	0.622	0.997
	39	0.427	2.632	–	0.047	−0.03	−0.7	0.271	0.603	0.999
	38.5	0.429	2.624	–	0.046	−0.029	−0.75	0.319	0.601	0.998
	38	0.424	2.686	–	0.05	−0.032	−0.826	0.4	0.609	0.986
	37.5	0.426	2.678	–	0.049	−0.031	−0.89	0.462	0.606	0.989

Table 6
Non-linear regression fit coefficients for factors influencing oil temperature of the tank's windward side.

Wind speed, m/s	Radius, m	Random error	Power	Wind speed at tank wall	Ambient temperature	Solar radiation	Density	Viscosity	Specific heat capacity	R^2
0.9	40	0.34	0.479	−7.466	−0.248	−0.224	7	0.4	0.992	0.979
	39.5	0.5	0.985	−6	−0.2	−0.199	5.229	0.5	0.787	0.992
	39	−1.515	0.681	−5	−0.2	−0.1	6	0.6	2.725	0.985
	38.5	−3.642	0.707	−5	−0.2	−0.1	8	0.7	4.855	0.991
	38	0.774	1.395	0.014	0.013	0.005	−0.663	−0.142	0.222	0.996
	37.5	0.75	0.967	0.04	0.008	0.004	1.488	−2.304	0.246	0.989
0.5	40	0.536	3	−0.6	0.061	−0.025	0.2	−0.208	0.498	0.992
	39.5	0.893	1.051	−0.3	0.051	0.052	−0.625	−0.023	0.055	0.983
	39	0.907	1.05	−0.2	0.037	0.039	−0.699	−0.049	0.054	0.975
	38.5	−0.646	0.853	−0.1	−0.058	−0.061	0.7	0.1	1.708	0.979
	38	−0.935	0.861	−0.1	−0.07	−0.07	1	0.1	2.005	0.994
	37.5	0.519	1.405	−0.096	0.004	0.002	1.313	−1.739	0.48	0.981
0	40	0.419	2.658	–	0.05	−0.032	−0.5	0.079	0.613	0.995
	39.5	0.4	3.042	–	0.074	−0.05	−1.374	0.972	0.65	0.991
	39	0.4	3.044	–	0.074	−0.05	−1.382	0.98	0.65	0.993
	38.5	0.368	2.885	–	0.075	−0.048	0.645	−1.017	0.68	0.985
	38	0.381	3.243	–	0.089	−0.062	−1.364	0.98	0.68	0.976
	37.5	0.376	3.307	–	0.094	−0.066	−1.368	0.99	0.69	0.986

factor in Fig. 12(c), indicating that the heat transfer mode with heat conduction between crude oil as the main and natural convection as the secondary is formed at the bottom of the tank without wind. In addition, a transition zone (II) with a thickness of 1.2–1.46 m of cold oil from the top temperature drop sinking along the tank wall is accumulated at the bottom of the tank.

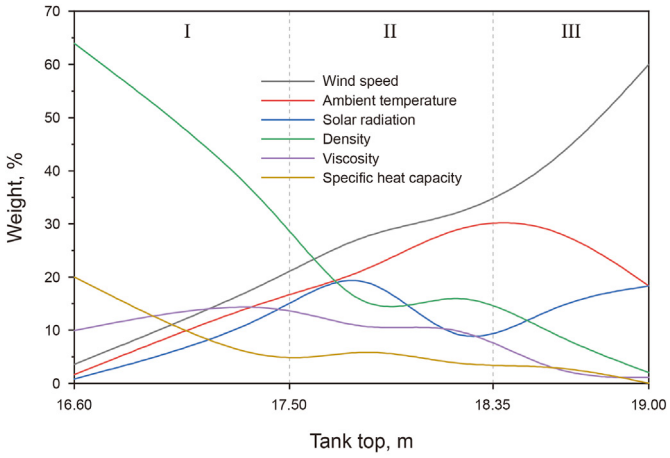

(a) Wind speed 0.9 m/s

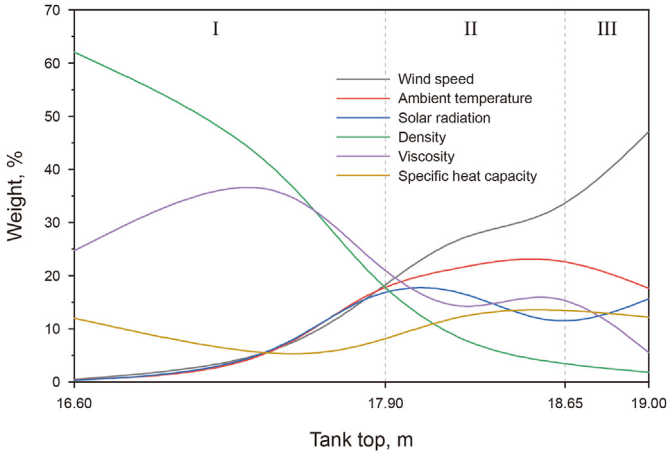

(b) Wind speed 0.5 m/s

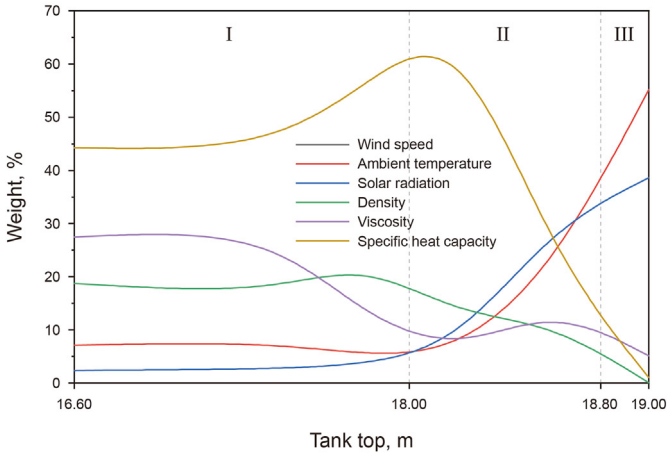

(c) Wind speed 0 m/s

Fig. 11. Weighting of factors influencing the temperature of the tank top.

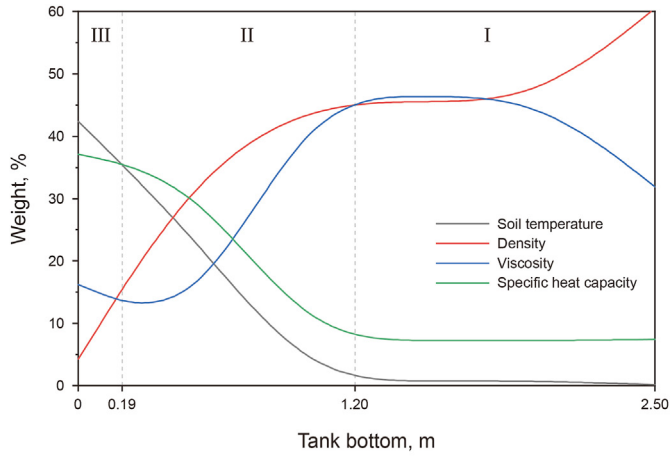

(a) Wind speed 0.9 m/s

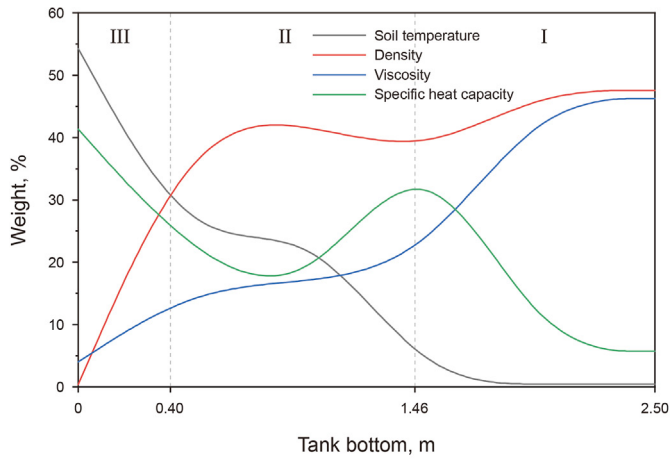

(b) Wind speed 0.5 m/s

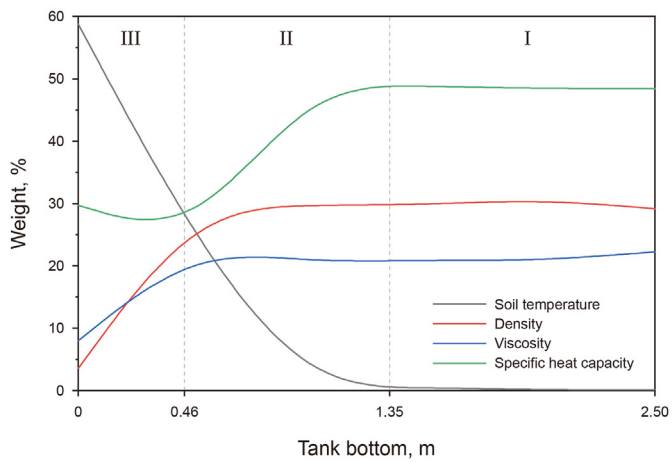

(c) Wind speed 0 m/s

Fig. 12. Weighting of factors influencing the temperature of the tank bottom.

As shown in Fig. 13(a) and (b), within the thickness of 0.91 and 0.28 m from the leeward side of the tank wall, and 0.72 and 0.24 m from the windward side of Fig. 14(a) and (b), an external influence zone (III) dominated by forced convection heat transfer with wind speed accounting for 30%–45% was formed. Near the center side of the tank, the crude oil is weakened by the forced convection of external wind speed, and gradually shifts from the external influence zone (III) dominated by forced convection to the transition zone (II) dominated by natural convection heat transfer caused by density difference, with wind speed being secondary. Finally, it enters the internal natural convection influence zone (I) with the thickness of 0.68–1.5 m dominated by crude oil physical properties.

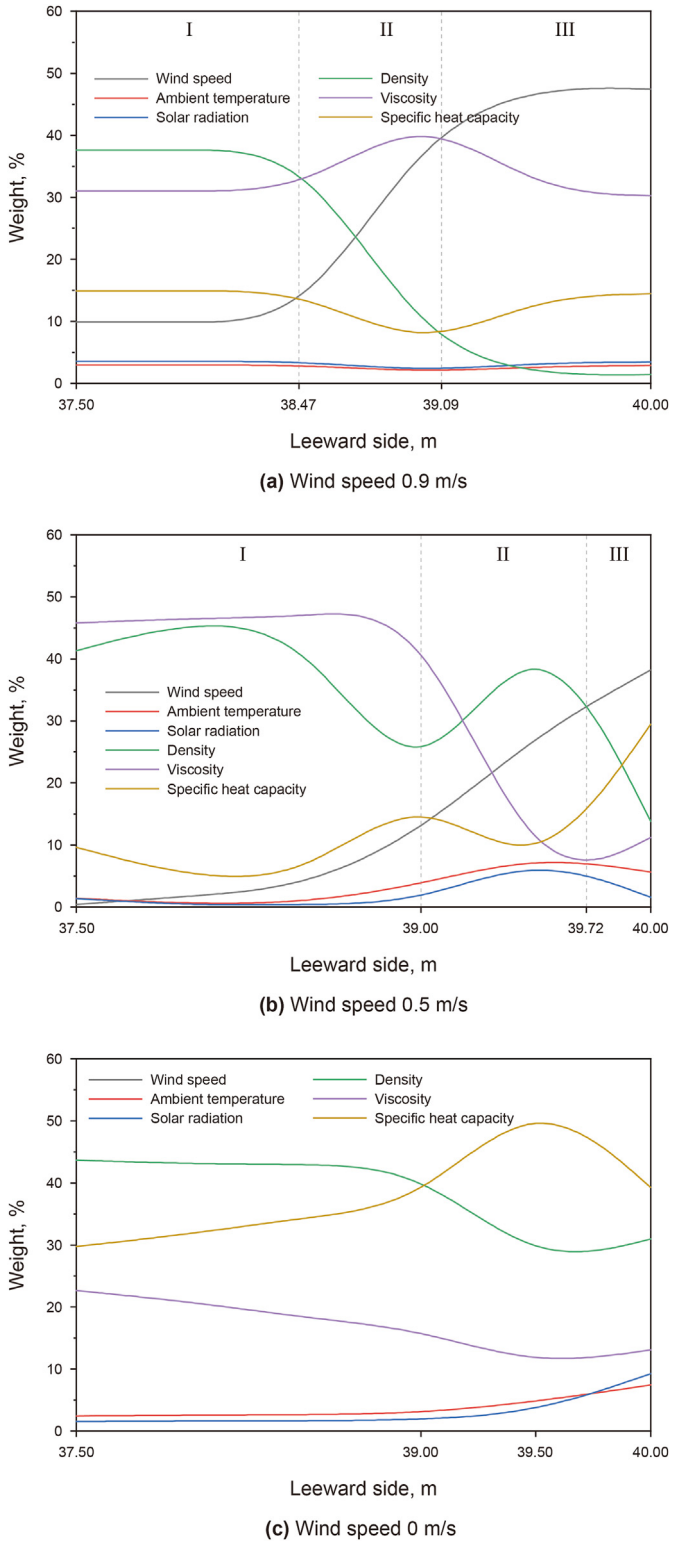

Fig. 13. Weighting of factors influencing the temperature of the tank's leeward side.

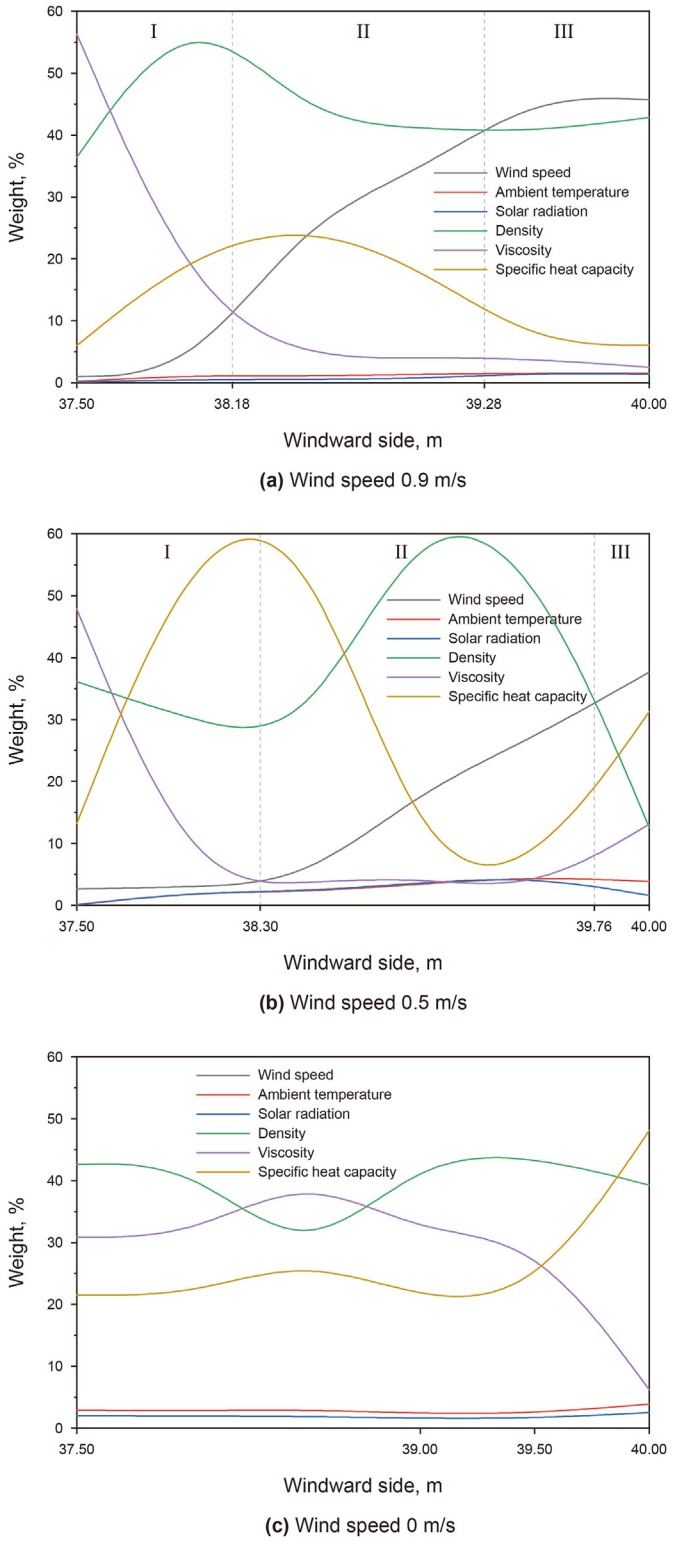

Fig. 14. Weighting of factors influencing the temperature of the tank's windward side.

Combining the weighting of the temperature influence factors of the windward side and leeward side boundaries of the three working conditions, it can be found that the larger the wind speed is, the larger the external influence zone is. The external influence zone on the windward side expands from 39.76–40 to 39.28–40 m, and the external influence zone on the leeward side expands from 39.72–40 to 39.09–40 m, while the transition zone becomes smaller and smaller instead, with the transition zone on the windward side narrowing from 38.3–39.76 to 38.18–39.28 m, and the transition zone on the leeward side narrowing from 39–39.72 to 38.47–39.09 m. Compared with the windward side, the external forced convection on the leeward side has more influence on the

temperature drop of crude oil. The external influence layer on the leeward side is 0.04–0.19 m thicker than that on the windward side, while the transition layer is 0.48–0.74 m thinner than that on the windward side, which further explains why the temperature change at the boundary between the tank wall and the top of the tank on the leeward side is significantly stronger than that on the windward side. Overall, with the change of wind speed from 0.5 to 0.9 m/s, the weight of ambient temperature and solar radiation decreased from 10.41% to 7.79%, indicating that the increase of wind speed at the tank wall would weaken the effect of ambient temperature and solar radiation on the temperature drop of crude oil.

5. Conclusions

This paper develops a theoretical model of the heat transfer process of non-steady state temperature drop in crude oil storage tank under coupled dynamic thermal environment conditions, analyses the influence law of crude oil temperature drop in storage tank under the coupling effect of external forced convection, thermal radiation, natural convection, and other heat transfer modes, and determines the different external dynamic thermal environment influence zone (III), internal crude oil physical property influence zone (I) and the transition zone (II). The weights of the ambient temperature, solar radiation, wind speed and crude oil density, viscosity, and specific heat capacity of the storage tank on each influence zone were also quantified.

(1) The heat transfer mode of the tank boundary was clarified. The tank wall is mainly based on convective heat transfer with the wind bypassing the column. Initially, the convective heat transfer on the windward side of the tank wall is stronger and the temperature drop is faster. But as time increases, the backwind side gradually forms an obvious turbulent vortex structure, which strengthens the convective heat transfer and enhances the heat transfer rate between the crude oil on the backwind side and the tank wall. And as the wind speed increases, the forced convection at the top of the tank is more obvious and the temperature drop is faster.

(2) The temperature fluctuations at the top and bottom of the tank as well as the tank wall space were analyzed. The crude oil near the top of the tank at 19 m has the lowest temperature, higher viscosity, and weaker fluidity; when the level is lowered to 16.6 m the temperature tends to stabilize, indicating that the oil in this area is less affected by the external environment. The temperature fluctuation near the bottom of the tank is more obvious, the fluctuation of 0.5–1.5 m reaches 0.15 °C, while the temperature of 2–2.5 m basically tends to be stable, and the oil temperature of 0–0.5 m near the soil at the bottom of the tank is lower. The overall temperature change between the leeward and windward sides of the tank wall is small due to the effect of the insulation layer. The oil temperature is lowest at 40 m from the external environmental boundary.

(3) A multiple non-linear regression method was used to quantitatively characterize the weights of the external ambient temperature of the tank, solar radiation, wind speed, and internal crude oil density, viscosity, and specific heat capacity of the tank on the temperature drop of crude oil in each influencing region. The wind swept through the flat plate near the tank level of 19 m to form the external environmental influence zone (III) with forced convection as the main influence, supplemented by solar radiation and ambient temperature conduction, and the total external conditions accounted for over 70%, with wind speed as the main influence factor accounting for nearly 50% of the weight. When the liquid level drops to 17.5 and 17.9 m respectively, the area is the internal influence zone (I), where crude oil density is the main influence factor and natural convection is the main heat transfer method. An external soil influence zone (III) with a thickness of 0.19–0.46 m is formed at the bottom of the tank, with a soil temperature influence weighting of 40%–60%. On the leeward and windward sides of the tank wall, an external influence zone (III) is formed, where forced convection is the main heat transfer mode, with wind speed accounting for 30%–40%. The crude oil near the center of the tank is weakened by the forced convection of external wind speed, and gradually shifts from the external environmental influence zone (III), where forced convection is the main influence, to the internal natural convection influence zone (I), where the physical properties of the crude oil are the main influence. At the same time, the weighting of the influence of ambient temperature and solar radiation decreases with increasing wind speed, indicating that the wind speed at the tank wall weakens the influence of ambient temperature and solar radiation on the temperature drop of crude oil.

Decalaration of competing interest

We declare that we have no financial and personal relationships with other people or organizations that can inappropriately influence our work, there is no professional or other personal interest of any nature or kind in any product, service and/or company that could be construed as influencing the position presented in, or the review of, the manuscript entitled, “Study of main factors influencing unsteady-state temperature drop in oil tank storage under dynamic thermal environment coupling”.

Acknowledgements

This work was financially supported by the National Natural Science Foundation of China (52104064) (52074089), the China Postdoctoral Science Foundation (2020M681074), Heilongjiang Provincial Natural Science Foundation of China (YQ2023E006), University Nursing Program for Young Scholars with Creative Talents in Heilongjiang Province (UNPYSCT-2020152), Postdoctoral Science Foundation of Heilongjiang Province in China (LBH-TZ2106) (LBH-Z20122), Northeast Petroleum University Talents Introduction Fund (2019KQ18).

References

British Petroleum, 2021. BP Statistical Review of Word Energy.

Cotter, M.A., Charles, M.E., 1993. Transient cooling of petroleum by natural convection in cylindrical storage tanks—II. Effect of heat transfer coefficient, aspect ratio and temperature-dependent viscosity. Int. J. Heat Mass Tran. 36 (8), 2175–2185. https://doi.org/10.1016/s0017-9310(05)80148-6.

Huang, W., Chen, F., Lv, C., et al., 2020. Numerical simulation of oil and gas leakage dispersion from internal floating roof tanks based on wind tunnel platform experiments. Oil Gas Storage Transp. 39 (4), 425–433. https://doi.org/10.6047/j.issn.1000-8241.2020.04.010 (in Chinese).

Kocijel, L., Mrzljak, V., Glažar, V., 2020. Numerical analysis of geometrical and process parameters influence on temperature stratification in a large volumetric heat storage tank. Energy 194, 116878. https://doi.org/10.1016/j.energy.2019.116878.

Li, H., Rong, L., Zhang, G., 2016. Study on convective heat transfer from pig models by CFD in a virtual wind tunnel. Comput. Electron. Agric. 123, 203–210. https://doi.org/10.1016/j.compag.2016.02.027.

Li, W., Shao, Q., Liang, J., 2019. Numerical study on oil temperature field during long storage in large floating roof tank. Int. J. Heat Mass Tran. 130, 175–186. https://doi.org/10.1016/j.ijheatmasstransfer.2018.10.024.

Lin, W., Armfield, S.W., 2005. Long-term behavior of cooling fluid in a vertical cylinder. Int. J. Heat Mass Tran. 48 (1), 53–66. https://doi.org/10.1016/j.ijheatmasstransfer.2004.07.038.

Liu, C.H., Chung, T.N.H., 2012. Forced convective heat transfer over ribs at various

separation. Int. J. Heat Mass Tran. 55 (19–20), 5111–5119. https://doi.org/10.1016/j.ijheatmasstransfer.2012.05.012.
Liu, J., Zhao, J., Si, M., et al., 2019. The effect of periodic change of external temperature on the temperature field of crude oil. Case Stud. Therm. Eng. 15, 100526. https://doi.org/10.1016/j.csite.2019.100526.
Liu, J., Zhao, J., Si, M., et al., 2020. Effect of periodic change of ambient temperature on the temperature field in the single disc floating roof oil tank. Journal of Applied Science and Engineering 23 (1), 129–142. https://doi.org/10.6180/jase.202003_23(1).0014.
Pasley, H., Clark, C., 2000. Computational fluid dynamics study of flow around floating-roof oil storage tanks. J. Wind Eng. Ind. Aerod. 86 (1), 37–54. https://doi.org/10.1016/s0167-6105(99)00138-5.
Seddegh, S., Wang, X., Henderson, A.D., 2015. Numerical investigation of heat transfer mechanism in a vertical shell and tube latent heat energy storage system. Appl. Therm. Eng. 87, 698–706. https://doi.org/10.1016/j.applthermaleng.2015.05.067.
Sun, W., Cheng, Q., Zheng, A., et al., 2018. Research on coupled characteristics of heat transfer and flow in the oil static storage process under periodic boundary conditions. Int. J. Heat Mass Tran. 122, 719–731. https://doi.org/10.1016/j.ijheatmasstransfer.2018.02.010.
Sun, W., Liu, Y., Li, M., et al., 2023. Study on heat flow transfer characteristics and main influencing factors of waxy crude oil tank during storage heating process under dynamic thermal conditions. Energy 269, 127001. https://doi.org/10.1016/j.energy.2023.127001.
Wang, M., Zhang, X., Shao, Q., et al., 2019. Temperature drop and gelatinization characteristics of waxy crude oil in 1000 m^3 single and double-plate floating roof oil tanks during storage. Int. J. Heat Mass Tran. 136, 457–469. https://doi.org/10.1016/j.ijheatmasstransfer.2019.02.082.
Wang, M., Zhang, Y., Cao, W., 2005. Temperature drop pattern of vertical floating roof crude oil storage tanks. Gasf. Surf. Eng. 12, 11–12. CNKI:SUN:YQTD.0.2005-12-009.
Wang, Q., Song, X., 2019. Forecasting China's oil consumption: a comparison of novel nonlinear-dynamic grey model (GM), linear GM, nonlinear GM and metabolism GM. Energy 183, 160–171. https://doi.org/10.1016/j.energy.2019.06.139.
Wang, Y., Lin, M., 2020. Numerical simulation on oil spilling of submarine pipeline and its evolution on sea surface. Comput. Model. Eng. Sci. 124 (3), 885–914. https://doi.org/10.32604/cmes.2020.09810.
Wang, Y., Wang, B., Liu, Y., et al., 2020. Study on asymmetry concentration of mixed oil in products pipeline. Energies 13 (23), 6398. https://doi.org/10.3390/en13236398.
Wang, Y., Yu, B., Sun, S., 2012a. Fast prediction method for steady-state heat convection. Chem. Eng. Technol. 35 (4), 668–678. https://doi.org/10.1002/ceat.201100428.
Wang, Y., Yu, B., Cao, Z., et al., 2012b. A comparative study of POD interpolation and POD projection methods for fast and accurate prediction of heat transfer problems. Int. J. Heat Mass Tran. 55 (17–18), 4827–4836. https://doi.org/10.1016/j.ijheatmasstransfer.2012.04.053.
Wilamowski, B.M., Irwin, J.D., 2018. Intelligent Systems. CRC Press.
Xue, W., Wang, Y., Chen, Z., et al., 2023. An integrated model with stable numerical methods for fractured underground gas storage. J. Clean. Prod. 393, 136268. https://doi.org/10.1016/j.jclepro.2023.136268.
Zhang, Z., Cui, G., Xu, C., 2008. Theory and Application of Numerical Simulation of Turbulent Large Eddies. Tsinghua University Press (in Chinese).
Zhao, J., Dong, H., Wang, X., et al., 2017. Research on heat transfer characteristic of crude oil during the tubular heating process in the floating roof tank. Case Stud. Therm. Eng. 10, 142–153. https://doi.org/10.1016/j.csite.2017.05.006.
Zhao, J., Liu, J., Dong, H., et al., 2020. Numerical investigation on the flow and heat transfer characteristics of waxy crude oil during the tubular heating. Int. J. Heat Mass Tran. 161, 120239. https://doi.org/10.1016/j.ijheatmasstransfer.2020.120239.
Zhao, J., Liu, Y., Wei, L., et al., 2014. Transient cooling of waxy crude oil in a floating roof tank. J. Appl. Math. 2014, 1–12. https://doi.org/10.1155/2014/482026.